

# Hybrid Flexible NFC Sensor on Paper

Silvia Conti<sup>1</sup>, Francesco Nepa<sup>1</sup>, Stefano Di Pascoli<sup>1</sup>, Irene Brunetti<sup>1</sup>, Lorenzo Pimpolari, Xiuju Song, Khaled Parvez, Hamed Javanbakht Lomeri<sup>1</sup>, Francesca De Rossi<sup>1</sup>, Giulia Lucarelli, Giuseppina Polino, Thomas Brown<sup>1</sup>, Laura Ferrer Pascual, María del Pilar Bernícola, Elena del Corro<sup>1</sup>, Enrique Gonzalez Marin, Sandy Sanchez, Anders Hagfeldt, Christian Callegari, Francesco Pieri<sup>1</sup>, Massimo Macucci, Michele Massaro, Giuseppe Iannaccone<sup>1</sup>, *Fellow, IEEE*, Jose Antonio Garrido, Francesca Brunetti, *Member, IEEE*, Cinzia Casiraghi, and Gianluca Fiori

**Abstract**—Everyday healthcare objects have become the focus of interdisciplinary research lines, which aim to monitor human biomedical parameters by means of ergonomic and, ideally, environmentally sustainable sensors. Here, a hybrid system, based on both solution-processed- and conventional silicon-technology, is reported. In particular, a strain and a pH sensor are developed based on graphene inks, while a humidity detector is implemented using a poly(3,4-ethylenedioxythiophene)–

poly(styrenesulfonate) (PEDOT:PSS). The printed sensors are integrated into a demonstrator consisting of a silicon near field communication (NFC) transponder chip with logic and transceiver capabilities, bonded on a circuit board with inkjet-printed components on a paper substrate: an antenna and a power supply (in addition to the sensor). This proof-of-concept seeks to address the needs for a future circular economy, as well as those for cheap, flexible, and lightweight, multi-functional electronics.

Manuscript received 29 December 2022; accepted 12 January 2023. Date of publication 20 January 2023; date of current version 25 April 2023. This work was supported by the H2020 Project WASP under Contract 825213. The work of Hamed Javanbakht Lomeri, Francesca De Rossi, Giulia Lucarelli, Giuseppina Polino, Thomas Brown, and Francesca Brunetti was supported by the European Union’s Horizon 2020 Research and Innovation Programme through Grant Agreement APOLO under Contract 763989. (*Silvia Conti and Francesco Nepa contributed equally to this work.*) (*Corresponding author: Francesco Nepa.*)

Silvia Conti was with the Dipartimento di Ingegneria dell’Informazione, University of Pisa, 56122 Pisa, Italy. She is now with the Plasmon Nanotechnologies, Istituto Italiano di Tecnologia, 16163 Genoa, Italy.

Francesco Nepa, Francesco Pieri, Massimo Macucci, and Gianluca Fiori are with the Dipartimento di Ingegneria dell’Informazione, University of Pisa, 56122 Pisa, Italy (e-mail: francesco.nepa@phd.unipi.it).

Stefano Di Pascoli and Giuseppe Iannaccone are with the Dipartimento di Ingegneria dell’Informazione, University of Pisa, 56122 Pisa, Italy, and also with Quantavis s.r.l., 56122 Pisa, Italy.

Irene Brunetti was with the Dipartimento di Ingegneria dell’Informazione, University of Pisa, 56122 Pisa, Italy. She is now with InnovationLab GmbH, 69115 Heidelberg, Germany.

Lorenzo Pimpolari was with the Dipartimento di Ingegneria dell’Informazione, University of Pisa, 56122 Pisa, Italy. He is now with the Institut de Microelectrònica de Barcelona IMB-CNM (CSIC), 08193 Barcelona, Spain.

Xiuju Song, Khaled Parvez, and Cinzia Casiraghi are with the Department of Chemistry, University of Manchester, M13 9PL Manchester, U.K.

Hamed Javanbakht Lomeri, Francesca De Rossi, Giulia Lucarelli, Giuseppina Polino, Thomas Brown, and Francesca Brunetti are with the Centre for Hybrid and Organic Solar Energy (CHOSE), Department of Electronic Engineering, University of Rome Tor Vergata, 00133 Rome, Italy.

Laura Ferrer Pascual, María del Pilar Bernícola, and Elena del Corro are with the Catalan Institute of Nanoscience and Nanotechnology (ICN2), CSIC, BIST, 08193 Barcelona, Spain.

Enrique Gonzalez Marin is with the Departamento de Electronica y Tecnología de Computadores, Facultad de Ciencias, Universidad de iGranada, 18071 Granada, Spain.

Sandy Sanchez and Anders Hagfeldt are with the Laboratory of Photomolecular Science (LSPM), École Polytechnique Fédérale de Lausanne (EPFL), 1015 Lausanne, Switzerland.

Christian Callegari is with Quantavis s.r.l., 56122 Pisa, Italy.

Michele Massaro is with Essity S.p.A., 55016 Lucca, Italy.

Jose Antonio Garrido is with the Catalan Institute of Nanoscience and Nanotechnology (ICN2), CSIC, BIST, 08193 Barcelona, Spain, and also with the Institut Català de Recerca i Estudis Avançats (ICREA), 08010 Barcelona, Spain.

This article has supplementary downloadable material available at <https://doi.org/10.1109/JFLEX.2023.3238682>, provided by the authors.

Digital Object Identifier 10.1109/JFLEX.2023.3238682

**Index Terms**—Graphene, humidity, near field communication (NFC) sensor, paper substrate, pH, poly(3,4-ethylenedioxythiophene)–poly(styrenesulfonate) (PEDOT:PSS), strain.

## I. INTRODUCTION

IN THE last 20 years, joint efforts from different research areas (including chemistry, physics, electronics, and medical engineering) have led to the development of flexible and conformable devices that lay at the core of Internet-of-Things systems in healthcare, sport, well-being as well as environmental monitoring [1], [2]. In this article, due to their wide range of applications, sensors that can detect changes in pressure, pH, and humidity levels are likely the most studied [3].

In particular, strain sensors are intensively investigated for their skin-like features in robotic and prosthetic systems [4], or to detect human motions [5], but are also exploited for structural health monitoring [6]. pH sensors, on the other hand, give information about the thermodynamics and kinetics of a variety of processes, and are fundamental in fields from metabolism and nutrition [7], to catalysis and pharmaceutical chemistry [8], from food manufacturing and processing [9] to environmental science [10]. Lastly, humidity sensors are crucial in the monitoring and control of the climate environment, in the semiconductor and food processing industries, as well as for medical applications [11], [12], [13].

The aforementioned uses have lifecycles ranging, on average, from hours to months, evidencing that the use of sustainable materials is a relevant necessity. In this arena, the paper highlights a cost-effective, recyclable alternative to plastic substrates [14]. Being compatible with high-speed roll-to-roll processes, it could play a role in reducing electronic waste at the global level [15], [16]. A good testbed to examine the potential of paper substrates are everyday objects such as bandages, hygiene products, or kitchen paper, that would, in this way, become “intelligent,” acquiring new features

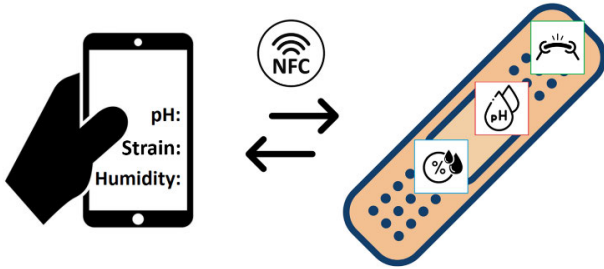


Fig. 1. Hybrid flexible transponder. Scheme of the NFC sensor transponder for measuring physical and chemical quantities. The reader is a common smartphone with NFC capabilities, with a reading range of the order of centimeters.

and being capable of monitoring biological, chemical, and physical parameters. To make these devices “user friendly,” their sensing functionalities have to be deployed on the objects, and the computation has to be performed in part directly on the objects, and in part in the cloud.

Here, a paper-based hybrid demonstrator with a near-field communication (NFC) silicon transponder chip and resistor-type sensors to detect pressure, pH, and humidity variations is presented. The concept is schematically illustrated in Fig. 1. The device can communicate with a standard smartphone with NFC capabilities with a reading range in the order of centimeters. The system is powered either through the NFC reader (passive mode) or through a flexible perovskite solar mini-module (FPSM), purposely devised for the transponder (active mode). Two different graphene-based printed resistors are employed for the strain and the pH sensors, whilst a poly(3,4-ethylenedioxythiophene)-poly(styrenesulfonate) (PEDOT:PSS) ink is employed to print the humidity detector. Having chosen paper as the substrate, resistor-based devices are adopted for their simplicity in terms of working principle, fabrication, and readout mechanism. This allows obtaining responses without using a reference electrode (typically needed in transistor-based configurations), both simplifying the electronics and limiting the size of the device, which can thus more easily be integrated inside commercial hygiene products such as patches and sanitary napkins. With the same perspective, inkjet printing has been employed as the fabrication process: it allows the definition of precise structures at the micrometer scale on flexible substrates, while being a low-cost technique that can be scaled up to mass production with a large yield [17].

## II. METHODS

### A. Materials

PEL P60 (purchased from Printed Electronics Ltd.) paper, commercial copy paper and sanitary napkins, and spin-coated polyimide (purchased from Microchemicals) films were used as substrates. A commercial silver ink (Sigma-Aldrich, silver dispersion) was used to print the antenna and the connections. A graphene ink was used to print the strain gauge and the pH sensor. The preparation process can be found in Supplementary Information Section I and the full characterization of the material (lateral size and thickness distribution,

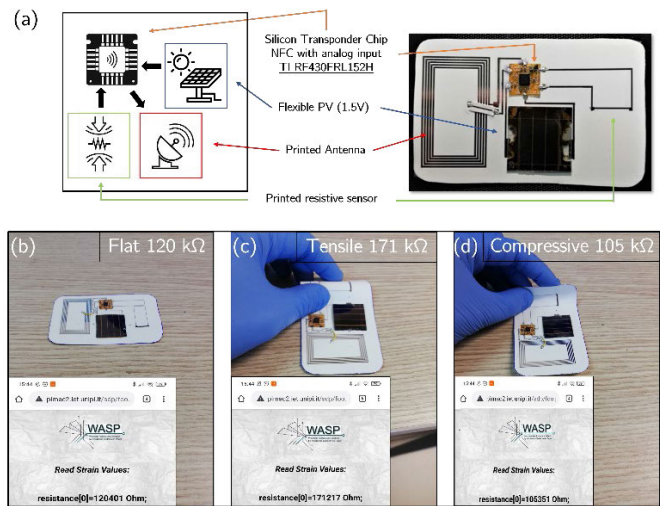


Fig. 2. Hybrid flexible strain sensor. (a) Scheme (left) and optical image (right) of the NFC strain sensor transponder. The transponder consists of a chip, an NFC transceiver, a printed graphene strain sensor, a printed perovskite solar cell, and a printed silver antenna. The system correctly displays the value of the resistance of the strain gauge without the application of (b) strain, or to (c) tensile or (d) compressive strain.

crystallinity, etc.) has already been presented in [18]. A commercial PEDOT:PSS ink (Heraeus Clevis<sup>1</sup>, PH1000) was modified with two different formulations and employed to print the humidity detectors. The first one (PEDOT:PSS/EG) was prepared by adding 5 mL of ethylene glycol (EG), 50  $\mu$ L of 4-dodecylbenzenesulfonic acid, and 1 wt% of 3-glycidoxypropyltrimethoxysilane (1 wt%) to 20 mL of the commercial ink. The second one (PEDOT:PSS/DMSO) was prepared with a 5 wt% of dimethyl sulfoxide (DMSO).

### B. Fabrication of the FPSMs

FPSMs are composed of a PET/ITO/SnO<sub>2</sub>/Perovskite/spiro-OMeTAD/Au structure (Supplementary Information Section II). The FPSMs layout is based on three cells connected in series with an overall active area of 2.3 cm<sup>2</sup> obtained by UV Nd:YVO<sub>4</sub> laser beam processing [19]. To define the width of the individual cells, the transparent conductive oxide (TCO) constituting the bottom electrode was linearly removed (laser patterning step 1, P1). Subsequently, all the layers of the module were deposited by spin-coating. The perovskite absorber and electron and hole transport layers (SnO<sub>2</sub> and Spiro-OMeTAD) were removed (laser patterning step, P2) beside the P1 scribe line to expose the TCO. Finally, the Au back contact electrode was ablated (laser patterning step, P3) next to the P2 scribe to electrically separate the sub-cells of the module. The module aperture ratio (AR) between the active area and the aperture area is approximately 87%. The JV characterization of the FPSMs is reported in the Supplementary Information (Fig. S1 and Table S1).

### C. Fabrication of the NFC sensor

The hybrid flexible NFC sensor, shown in Fig. 2(a), is fabricated on PEL P60. At first, the antenna and the connections

<sup>1</sup>Trademarked.

to the sensor and the power supply were inkjet-printed on the paper substrate using a Dimatix 2850 inkjet printer, depositing three consecutive layers of silver ink, with one nozzle of a 10 pL cartridge, a drop spacing of 40  $\mu\text{m}$ , and keeping the printer platen and the cartridge at room temperature. The substrate is then annealed at 110  $^{\circ}\text{C}$  for 30 min on a hot plate. The final resistance of the antenna is around 30  $\Omega$ . Finally, the NFC transponder (TI RF430FRL152H, based on a Texas Instrument Tag) as well as the passive components (resistances and capacitors) are soldered on a flexible PCB (12  $\times$  12 mm and thickness 50  $\mu\text{m}$ ) and glued to the paper substrate.

The resistive sensor can communicate with a smartphone through the silicon NFC transponder chip with custom firmware developed in C language. The resistance value is sampled by a 14-bit  $\Sigma\Delta$  analog-to-digital converter (ADC) and then transferred to a standard tag reader integrated into a common smartphone, which collects the measured data. The transponder writes the data into an NFC data exchange format (NDEF), like a uniform resource locator (URL) string, and includes the raw sensor data into the URL file path itself. For a given URL, the default operation consists of opening the URL with a web browser. The web browser communicates with the web server so that the PHP script extracts the raw voltage data embedded in the URL, calculates the corresponding physical values, and generates a web page with the formatted data ready to be read by the user.

In particular, the value of the sensor resistance (as for the case of the considered resistive sensors, i.e., strain, pH, and humidity sensors) is converted to the quantity of interest to be detected, through a purposely devised lookup table, depending on the type of the adopted sensor.

A mobile application has been developed to collect sensor data through a mobile phone. It has been made available for free on Google Play Store under the name of WASP Reader.

#### D. Fabrication of Graphene Resistors for Strain Sensors

Graphene electrodes were deposited between inkjet-printed silver interconnections on a PEL P60 paper substrate. In particular, the electrodes were printed by depositing five layers of graphene ink using one nozzle of a 10 pL cartridge, a drop spacing of 20  $\mu\text{m}$ , and keeping the printer platen and the cartridge at room temperature. The sensor has a rectangular area of 10  $\times$  0.5 mm, as shown in Fig. 3(a). The sensors were annealed at 110  $^{\circ}\text{C}$  for 10 min on a hot plate. Their final resistance is around 120 k $\Omega$ . The detailed characterization of the graphene strain gauges is reported in [20].

#### E. Fabrication of Graphene Resistors for pH Sensing

Graphene electrodes were printed between gold electrodes evaporated on polyimide substrates. Apart from the contact area, the gold electrodes are passivated with a polyimide film to avoid direct contact with the solutions. Graphene electrodes were fabricated by printing 10-, 20- and 30-layer passes, using one nozzle of a 10 pL cartridge, a drop spacing of 20  $\mu\text{m}$ , and keeping the platen and the cartridge at room temperature. The sensor has a rectangular area of 1.5  $\times$  0.6 mm as shown

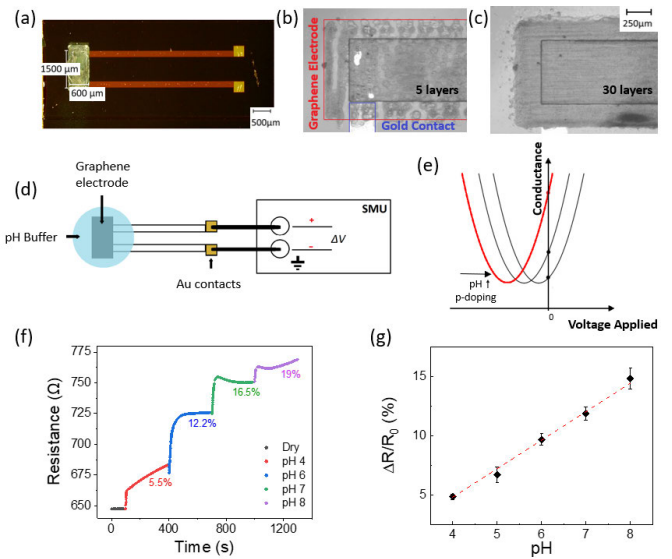


Fig. 3. Graphene electrodes as pH sensors. (a) Graphene electrode with gold contacts on polyimide substrate. (b) and (c) Optical images of a graphene electrode prototype during the fabrication process. The number of printing layers increases from (b) 5 to (c) 30 in. (d) Schematic of the pH measurement system. (e) Monotonic increasing trend in the resistance measurements. (f) Real-time resistance measurements of the graphene sensor when exposed to pH buffers from pH 4 to 9. (g) Average percentage variation (calculated over five electrodes for each pH point) with standard deviation error bars as a function of pH solution after the stabilization of the resistance. Linear regression line is also shown.

in Fig. 3(a). After the printing process, the electrodes were thermally annealed in vacuum at 350  $^{\circ}\text{C}$  for 1 h.

#### F. Fabrication of PEDOT:PSS Resistors for Humidity Detection

PEDOT:PSS electrodes were fabricated on a commercial copy paper by printing 10-, 15-, and 20-layer passes, using one nozzle of a 10 pL cartridge, a drop spacing of 20  $\mu\text{m}$ , and keeping the platen and the cartridge at room temperature. The sensor has a rectangular area of 6  $\times$  1.6 mm as shown in Fig. 4(c). For both formulations (see Materials), after the printing process, the electrodes were thermally annealed on a hot plate at 120  $^{\circ}\text{C}$  for 30 min.

#### G. Electrical Characterization

All the electrical measurements have been performed under ambient conditions. The resistance of the graphene and PEDOT:PSS electrodes were measured in a two-point-probe configuration using a Keithley SCS4200 parameter analyzer. Current density/voltage (JV) characterization of the FPSMs was performed using a Sun simulator (1 sun) and the LED light of the smartphone's torch (1000 lx). The detailed characterization is reported in the Supplementary Information Section II.

#### H. Bending Characterization

All the measurements were carried out by attaching the electrode to either the outer or inner surface of a cylinder. Four cylinders with different curvature radii (0.6, 2, 3, and 5.5 cm) were used.

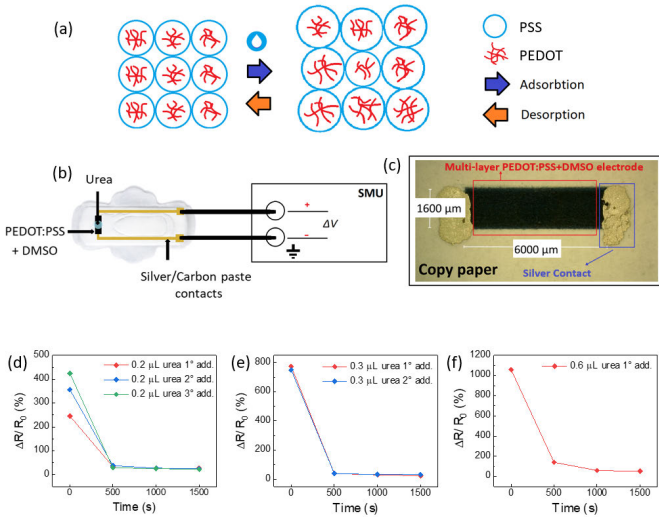


Fig. 4. Characterization of the PEDOT:PSS electrodes as humidity detectors. (a) Schematic of water adsorption and desorption in PEDOT:PSS film. (b) Schematic of the humidity measurement system. (c) Optical image of 15-layer PEDOT:PSS/DMSO electrode printed on copy paper. (d)–(f) Resistance percentage variation over time with different urea drop volumes, for 15-layer PEDOT:PSS/DMSO electrodes. (c) Red diamonds correspond to a first addition of 0.2  $\mu\text{L}$  of urea onto the electrode, the blue diamonds to a second addition of 0.2  $\mu\text{L}$  of urea, and the green diamonds to a third addition of 0.2  $\mu\text{L}$  of urea to get a final volume of 0.6  $\mu\text{L}$ . (d) Red diamonds correspond to a first addition of 0.3  $\mu\text{L}$  of urea onto the electrode, and the blue diamonds to a second addition of 0.3  $\mu\text{L}$  of urea to get a final volume of 0.6  $\mu\text{L}$ . (e) Red diamonds refer to the addition of a single 0.6  $\mu\text{L}$  urea drop.

### III. RESULTS AND DISCUSSION

#### A. Graphene resistors for strain sensing

As a first demonstration of the potential of the proposed approach, a graphene strain gauge, developed by part of Casiraghi et al. [20] was integrated into the hybrid flexible transponder. The demonstrator is shown in Fig. 2(a). In particular, five layer-graphene strain gauges were inkjet-printed on a paper substrate and employed as the sensor (see Methods for details) while the NFC silicon transponder chip as well as the passive components were soldered on a flexible PCB. The connections to the sensor and the power supply, as well as the antenna, were inkjet-printed on the same paper substrate using silver-based ink. The power supply was provided by an FPSM structure fabricated on a polyimide substrate (see Methods and Supplementary Information Section II for details). The sensor can communicate with a smartphone through NFC protocol (see the fabrication of the NFC sensors for details). In addition to the active mode, which includes a power supply (such as a button battery and PVC cell, etc.), a passive mode has also been implemented by exploiting wireless power transfer from the NFC reader itself.

As shown in the bottom part of Fig. 2, the system manages to read and display the value of the resistance of the strain gauge without the application of any strain [Fig. 2(b), 120 k $\Omega$ ], or when a tensile [Fig. 2(c), 171 k $\Omega$ ] or a compressive [Fig. 2(d), 105 k $\Omega$ ] strain is applied: a tensile strain leads to an increase of the resistance of the electrode, whilst an opposite behavior is detected for a compressive strain (for more details see Fig. S2). The results in Fig. 2 were obtained in passive

mode. The video in the Supplementary Information also shows the results obtained in the active mode using the PVC cell.

#### B. Graphene resistors for pH sensing

The pH sensor prototype consists of a graphene electrode printed between two evaporated gold contacts [Fig. 3(a)] on a flexible polyimide substrate (see Supplementary Information Section III and Methods for details). The main reason for the choice of polyimide as a substrate is the possibility to carry out multiple measurements of changing pH in real time. Fig. 3(b) and (c) shows the optical pictures captured by the printer fiducial camera during the fabrication process: the number of layers was increased from 5 [Fig. 3(b)] to 30 [Fig. 3(c)] with a five-layer step (i.e., during the fabrication process, the surface was flipped every five layers to achieve homogeneous surface profiles). In Fig. 3(b), the graphene electrode and gold contact areas are highlighted by red and blue lines, respectively. Three sets of electrodes were fabricated, with an increasing number of layers: 10, 20, and 30. The cleanliness of the graphene surface is important for the sensor to work correctly. Thus, a thermal annealing process (vacuum at 350  $^{\circ}\text{C}$  for 1 h) was introduced to remove fabrication residues and impurities and obtain highly conductive films. After the annealing process, the average resistances decrease by two orders of magnitude with respect to the strain gauge ones reported in the previous paragraph (see Table S2 and Fig. S3 in the Supplementary Information for details). Fig. 3(d) shows the schematic of the pH measurement setup. From a previous characterization, 20 it is known that the graphene ink employed in this work is n-type doped [red curve in Fig. 3(e)]. The surface-adsorbed ions in alkaline solutions are primarily hydroxyl ions ( $\text{OH}^-$ ), which partially repulse the electrons (majority carriers) from the graphene film, leading to a right shift of the conductance curves [21], [22]. Thus, for a reference voltage in the n-branch of the  $I$ - $V$  curve [e.g., 0 V in Fig. 3(e)] the conductance decreases when the pH value increases. We first tested the system in real-time to changes in pH values [Fig. 3(f)]. Initially, a drop of pH 4 solution was deposited and, subsequently, specific quantities of a NaOH solution (0.1 M) were added to increase the pH value on the electrode. Next, a second test was performed by depositing a 0.3  $\mu\text{L}$  drop of three different solutions with pH values of 4, 7, and 9 on the electrode, so that the electrode is completely covered by the droplet. After each exposure, the electrodes were carefully rinsed with distilled water. Fig. 3(g) shows the average of the resistance percentage variations with respect to the resistance of the dry electrode. Fig. S4 shows the variation of the electrode resistances as a function of the pH recorded after 500 s from exposure to the solution. Such a time interval is needed to guarantee a stable level of the current regardless of the pH value of the solution. The resistance increases with the pH value, as expected. When comparing the results obtained from devices printed with different numbers of layers (see Supplementary Information Section IV), it appears that the 30-layer electrodes show the smallest hysteresis. Moreover, they present the lowest resistance standard deviation and the lowest resistance values. For the reasons listed above, only the

30-layer electrodes were selected for the following tests. Five electrodes were used for each pH point, Table S3 shows the numerical values corresponding to the curve. The variation of the film resistance as a function of the pH of the buffer solution can be fit by

$$\frac{\Delta R}{R_0} = \frac{R - R_0}{R_0} = 0.024 \text{ pH} - 0.05$$

and from the above linear approximation, it results that the sensor sensitivity is equal to  $6.18 \text{ } \Omega/\text{pH}$  (where  $R_0$  is the resistance value in dry conditions,  $253 \text{ } \Omega$ ). This value is slightly lower than the ones previously reported for graphene-based pH sensors ( $17.5 \text{ } \Omega/\text{pH}$  [21] and  $30.8 \text{ } \Omega/\text{pH}$  [22], respectively), but it possesses a higher linearity (0.998 instead of 0.963). Furthermore, although flexible substrates were used in both cases, inkjet printing is definitely a more straightforward and reproducible fabrication process with respect to dielectrophoretic deposition and vacuum filtration. Comparable sensitivity values were obtained for printed single-walled carbon nanotubes (SWCNTs)-based pH sensors, but with a more complicated structure on a PDMS substrate ( $7.1 \text{ } \Omega/\text{pH}$ ) and using a screen-printing technique, which has a lower cost-efficiency ratio and is less environmentally friendly than inkjet-printing [23], [24].

### C. PEDOT:PSS electrodes for humidity sensing

Humidity tests were carried out employing two different PEDOT:PSS formulations onto three different paper-based substrates: copy paper, kitchen paper, and sanitary napkin. The two most commonly reported formulations for inkjet-printed PEDOT:PSS-based electrodes were chosen and compared [25]: PEDOT:PSS/EG and PEDOT:PSS/DMSO (see Methods). PEDOT:PSS is a water-absorbing material that can be exploited to implement humidity sensors. PEDOT:PSS films are characterized by a granular structure, where PEDOT-rich grains (conductive material) are surrounded by PSS (insulating, hydrophilic material). When humidity increases, a conductivity decrease of PEDOT:PSS is usually observed due to a drop in the electrical interconnections among PEDOT chains caused by water absorption (swelling) of PSS [Fig. 4(a)] [26]. With the idea of using these electrodes as humidity detectors in everyday life objects, like kitchen paper or sanitary towels, two different tests were carried out. The schematic of the humidity measurement setup is reported in Fig. 4(b). In the first one, fixed urea volumes were chosen to test the behavior of the electrodes in wetting conditions: 0.2, 0.3, and  $0.6 \text{ } \mu\text{L}$ . It is worth noting that the limited size of the electrode ( $6 \times 1.6 \text{ mm}$ ) required the use of small volumes of urea to avoid contact between the liquid and the silver paste used to contact the electrode ends. In the second test, the resistances were measured with the electrode bent onto cylinders of different radii (2, 3, and 5.5 cm) to check the bending effect on the electrode response, for both concave and convex configurations. First, tests were carried out on the PEDOT:PSS/EG electrodes (Fig. S6). From the results in Supplementary Information Section 5, it appears that it is impossible to discriminate between the wetting

and bending effects (see Fig. S7 and Fig. S8). As a consequence, this PEDOT:PSS ink was discarded for the prototype development. Fig. 4(c) shows the optical micrograph of a 15-layer PEDOT:PSS/DMSO electrode: the red line indicates the PEDOT:PSS/DMSO area and the blue line encloses the silver paste used to make the contacts. The average resistance of the 15-layer electrodes, before and after the annealing process, were  $(56.6 \pm 3.0) \text{ k}\Omega$  and  $(46.5 \pm 2.1) \text{ k}\Omega$ , respectively (average resistance values of the 10-, 15-, and 20-layer electrodes are shown in Fig. S9). Fig. 4(d)–(f) shows the response of the electrodes to different wetting conditions. In Fig. 4(d), the red points correspond to the first addition of a  $0.2 \text{ } \mu\text{L}$  urea drop on the electrode, while the blue points correspond to the second addition of a  $0.2 \text{ } \mu\text{L}$  urea drop on the same electrode. Eventually, to reach a total volume of  $0.6 \text{ } \mu\text{L}$ , a third addition of a  $0.2 \text{ } \mu\text{L}$  urea drop is performed, and the electrode response is shown with green points. In Fig. 4(e), the red points correspond to the first addition of a  $0.3 \text{ } \mu\text{L}$  urea drop on the electrode, while the blue points relate to the second addition of a  $0.3 \text{ } \mu\text{L}$  urea drop on the electrode, to reach a total volume of  $0.6 \text{ } \mu\text{L}$ . Fig. 4(f) refers to the addition of a single  $0.6 \text{ } \mu\text{L}$  urea drop. In the first two cases, the resistance increases to reach a peak after around 10 s from the deposition of the drop and then it stabilizes within 500 s. A larger time interval, up to 1000 s, is required for the  $0.6 \text{ } \mu\text{L}$  drop, which is probably due to the larger drop volume. As already underlined, the conduction in the conjugated polymer mainly relies on electron hopping among PEDOT chains, while the PSS chains are responsible for water absorption due to their hydrophilic properties. With the absorption of water molecules in the PSS chains, the distance between adjacent PEDOT chains increases. As a result, the hopping conduction is jeopardized by the increased humidity, resulting in a variation in the resistance of the electrode. To test the effect of bending on the electrode response, the electrodes were attached to cylinders of different radii (2, 3, and 5.5 cm) and both concave and convex configurations were considered. As from Fig. S10, it appears that resistance percentage variations due to the presence of a liquid are much larger than those caused by the bending action. Even when considering the smallest drop volume ( $0.2 \text{ } \mu\text{L}$ ), the resistance percentage variation after 10 s from the exposure to the solution is around 240%, which is almost two orders of magnitude larger than the maximum variation induced by the bending actions (3.1% for a cylinder radius of 5.5 cm). Thus, the bending-induced variations can be considered of the same order as those determined by measurement uncertainties related to instrumentation setup and silver-paste contact reliability, etc. In Fig. S11, the same tests are described for the 20-layer electrodes. Compared to the results obtained for 15-layer electrodes, it is noted that the current needs a longer time to stabilize. Moreover, due to the small percentage change in the resistance for the 20-layer electrodes with respect to the 15-layer electrodes, we opted for the 15-layer one, which is simpler to fabricate.

For the above reason, the following tests were performed on 15-layer sensors only, while embedding the sensor onto a sanitary napkin (see Supplementary Information Section 6). In particular, the humidity detector prototype

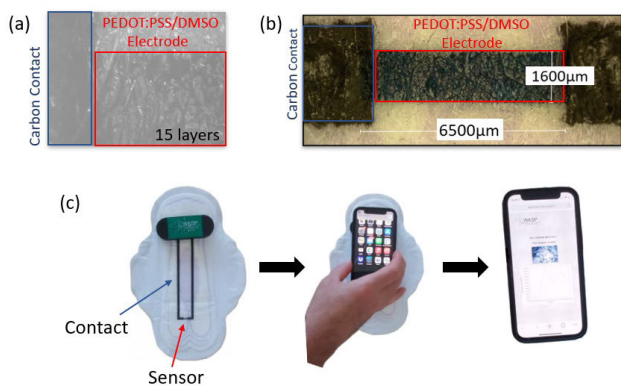


Fig. 5. Hybrid flexible humidity detector. (a) Optical image of a PEDOT:PSS/DMSO electrode during the printing process on sanitary napkin. (b) PEDOT:PSS/DMSO electrode with carbon paste contacts on sanitary napkin. (c) Integration of the humidity detector on sanitary napkin. The NFC transponder is interrupted by a smartphone with NFC technology. From the page that opens, it will be possible to check whether the sensor is wet or dry.

consists of a PEDOT:PSS/DMSO electrode printed between two screen-printed carbon paste contacts on a commercial sanitary napkin (Fig. 5 and Fig. S12). The contacts are 13 cm long and 0.4 cm wide, separated by 6 mm at the top, where the humidity sensor is printed (we have also considered the printing of the humidity sensor on kitchen papers, whose details can be found in the Supplementary Information, Fig. S13). Fig. 5(a) and (b) show captured optical pictures of a 15-layer PEDOT:PSS/DMSO electrode. Resistance tests with 0.2 and 0.3  $\mu\text{L}$  drop volumes showed quite low resistance percentage variation values. When a 0.6  $\mu\text{L}$  urea drop was added to the electrode, a 6% resistance increase was measured. The low percentage resistance variation with respect to what was obtained with the copy paper is probably related to the higher absorbency of the sanitary napkin, since they exhibit a multi-layer structure with different absorbency levels depending on the ad hoc application. The electrode was integrated into a system similar to the one employed in the case of the strain sensor. Fig. 5(c) shows the steps required to interrogate the sensor using a smartphone with NFC protocol. In this case, a button battery was used in order to log the values sampled by the sensor. The system can also be used in completely passive mode as the energy required by the microprocessor can be supplied by the smartphone through NFC communication (a real-time video is reported in the Supplementary Information).

#### IV. CONCLUSION

The design, fabrication, and characterization of three hybrid demonstrators for the detection of pressure, pH, and humidity levels, are presented. Graphene-based strain sensors are integrated with an NFC silicon transponder chip and an FPSM on paper. Graphene-based pH sensors, fabricated on a flexible polyimide substrate, have a sensitivity of 6.18  $\Omega/\text{pH}$  with a Pearson correlation coefficient of 0.998. PEDOT:PSS-based resistive humidity prototypes, fabricated copy paper, kitchen paper, and the sanitary napkin, show a sensitivity able to

obtain accurate and reliable humidity detectors which are robust with respect to the resistance variations induced by bending actions. These proof-of-concept devices are suitable for wearable applications on flexible substrates like polyimide and paper. Given their small size, they could be integrated into hygiene products and allow the monitoring of biomedical parameters.

#### ACKNOWLEDGMENT

Stefano Di Pascoli, Cinzia Casiraghi, Francesca Brunetti, and Gianluca Fiori conceived the idea. Silvia Conti, Stefano Di Pascoli, and Gianluca Fiori planned the experiments. Xiuju Song and Khaled Parvez prepared the graphene inks. Thomas Brown, Francesca De Rossi, Giulia Lucarelli, and Giuseppina Polino fabricated the solar cells. Silvia Conti, Francesco Nepa, Irene Brunetti, and Lorenzo Pimpolari performed the experiments and analyzed the data. Silvia Conti and Francesco Nepa wrote this article. All authors reviewed and contributed to this article.

#### REFERENCES

- [1] S. Huang, Y. Liu, Y. Zhao, Z. Ren, and C. F. Guo, "Flexible electronics: Stretchable electrodes and their future," *Adv. Funct. Mater.*, vol. 29, no. 6, pp. 1–15, 2019, doi: [10.1002/adfm.201805924](https://doi.org/10.1002/adfm.201805924).
- [2] J. Gao, K. Shang, Y. Ding, and Z. Wen, "Material and configuration design strategies towards flexible and wearable power supply devices: A review," *J. Mater. Chem. A*, vol. 9, no. 14, pp. 8950–8965, Apr. 2021, doi: [10.1039/D0TA11260G](https://doi.org/10.1039/D0TA11260G).
- [3] S. M. A. Iqbal, I. Mahgoub, E. Du, M. A. Leavitt, and W. Asghar, "Advances in healthcare wearable devices," *NPJ Flexible Electron.*, vol. 5, no. 1, p. 9, Apr. 2021, doi: [10.1038/s41528-021-00107-x](https://doi.org/10.1038/s41528-021-00107-x).
- [4] M. A. Rahman et al., "Artificial somatosensors: Feedback receptors for electronic skins," *Adv. Intell. Syst.*, vol. 2, no. 11, Nov. 2020, Art. no. 2000094, doi: [10.1002/aisy.202000094](https://doi.org/10.1002/aisy.202000094).
- [5] L. Tao et al., "Self-adapted and tunable graphene strain sensors for detecting both subtle and large human motions," *Nanoscale*, vol. 9, no. 24, pp. 8266–8273, 2017, doi: [10.1039/C7NR01862B](https://doi.org/10.1039/C7NR01862B).
- [6] J. Yan, A. Downey, A. Chen, S. Laflamme, and S. Hassan, "Capacitance-based sensor with layered carbon-fiber reinforced polymer and titania-filled epoxy," *Compos. Struct.*, vol. 227, Nov. 2019, Art. no. 111247, doi: [10.1016/j.compstruct.2019.111247](https://doi.org/10.1016/j.compstruct.2019.111247).
- [7] T. Grunhagen, G. Wilde, D. M. Soukane, S. A. Shirazi-Adl, and J. P. G. Urban, "Nutrient supply and intervertebral disc metabolism," *J. Bone Joint Surg.*, vol. 88, no. 2, pp. 30–35, Apr. 2006, doi: [10.2106/JBJS.E.01290](https://doi.org/10.2106/JBJS.E.01290).
- [8] M. Klinska, L. M. Smith, G. Gryn'ova, M. G. Banwell, and M. L. Coote, "Experimental demonstration of pH-dependent electrostatic catalysis of radical reactions," *Chem. Sci.*, vol. 6, no. 10, pp. 5623–5627, Sep. 2015, doi: [10.1039/C5SC01307K](https://doi.org/10.1039/C5SC01307K).
- [9] C. Bohnke, H. Duroy, and J.-L. Fourquet, "PH sensors with lithium lanthanum titanate sensitive material: Applications in food industry," *Sens. Actuators B, Chem.*, vol. 89, no. 3, pp. 240–247, Apr. 2003, doi: [10.1016/S0925-4005\(02\)00473-2](https://doi.org/10.1016/S0925-4005(02)00473-2).
- [10] S. Bhadra, D. S. Y. Tan, D. J. Thomson, M. S. Freund, and G. E. Bridges, "A wireless passive sensor for temperature compensated remote pH monitoring," *IEEE Sensors J.*, vol. 13, no. 6, pp. 2428–2436, Jun. 2013, doi: [10.1109/JSEN.2013.2255519](https://doi.org/10.1109/JSEN.2013.2255519).
- [11] K. M. Willett, N. P. Gillett, P. D. Jones, and P. W. Thorne, "Attribution of observed surface humidity changes to human influence," *Nature*, vol. 449, no. 7163, pp. 710–712, Oct. 2007, doi: [10.1038/nature06207](https://doi.org/10.1038/nature06207).
- [12] A. Rivadeneira, J. Fernández-Salmerón, M. Agudo, J. A. López-Villanueva, L. F. Capitan-Vallvey, and A. J. Palma, "Design and characterization of a low thermal drift capacitive humidity sensor by inkjet-printing," *Sens. Actuators B, Chem.*, vol. 195, pp. 123–131, May 2014, doi: [10.1016/j.snb.2013.12.117](https://doi.org/10.1016/j.snb.2013.12.117).
- [13] R. Liang, A. Luo, Z. Zhang, Z. Li, C. Han, and W. Wu, "Research progress of graphene-based flexible humidity sensor," *Sensors*, vol. 20, no. 19, p. 5601, Sep. 2020, doi: [10.3390/s20195601](https://doi.org/10.3390/s20195601).

- [14] W. Li et al., "Biodegradable materials and green processing for green electronics," *Adv. Mater.*, vol. 32, no. 33, Aug. 2020, Art. no. 2001591, doi: [10.1002/adma.202001591](https://doi.org/10.1002/adma.202001591).
- [15] D. Tobjörk and R. Österbacka, "Paper electronics," *Adv. Mater.*, vol. 23, no. 17, pp. 1935–1961, May 2011, doi: [10.1002/adma.201004692](https://doi.org/10.1002/adma.201004692).
- [16] H. Tai, Z. Duan, Y. Wang, S. Wang, and Y. Jiang, "Paper-based sensors for gas, humidity, and strain detections: A review," *ACS Appl. Mater. Interfaces*, vol. 12, no. 28, pp. 31037–31053, Jul. 2020, doi: [10.1021/acsami.0c06435](https://doi.org/10.1021/acsami.0c06435).
- [17] B. Derby, "Inkjet printing of functional and structural materials: Fluid property requirements, feature stability, and resolution," *Annu. Rev. Mater. Res.*, vol. 40, no. 1, pp. 395–414, Jun. 2010, doi: [10.1146/annurev-matsci-070909-104502](https://doi.org/10.1146/annurev-matsci-070909-104502).
- [18] D. McManus et al., "Water-based and biocompatible 2D crystal inks for all-inkjet-printed heterostructures," *Nature Nanotechnol.*, vol. 12, no. 4, pp. 343–350, Apr. 2017, doi: [10.1038/nnano.2016.281](https://doi.org/10.1038/nnano.2016.281).
- [19] B. Taheri et al., "Laser-scribing optimization for sprayed SnO<sub>2</sub>-based perovskite solar modules on flexible plastic substrates," *ACS Appl. Energy Mater.*, vol. 4, no. 5, pp. 4507–4518, May 2021, doi: [10.1021/acsaem.1c00140](https://doi.org/10.1021/acsaem.1c00140).
- [20] C. Casiraghi et al., "Inkjet printed 2D-crystal based strain gauges on paper," *Carbon*, vol. 129, pp. 462–467, Apr. 2018, doi: [10.1016/j.carbon.2017.12.030](https://doi.org/10.1016/j.carbon.2017.12.030).
- [21] P. Li, N. Lei, J. Xu, and W. Xue, "High-yield fabrication of graphene chemiresistors with dielectrophoresis," *IEEE Trans. Nanotechnol.*, vol. 11, no. 4, pp. 751–759, Jul. 2012, doi: [10.1109/TNANO.2012.2196524](https://doi.org/10.1109/TNANO.2012.2196524).
- [22] C.-Y. Lee, K. F. Lei, S.-W. Tsai, and N.-M. Tsang, "Development of graphene-based sensors on paper substrate for the measurement of pH value of analyte," *BioChip J.*, vol. 10, no. 3, pp. 182–188, Sep. 2016, doi: [10.1007/s13206-016-0304-7](https://doi.org/10.1007/s13206-016-0304-7).
- [23] J.-Y. Jeon, B.-C. Kang, and T.-J. Ha, "Flexible pH sensors based on printed nanocomposites of single-wall carbon nanotubes and Nafion," *Appl. Surf. Sci.*, vol. 514, Jun. 2020, Art. no. 145956, doi: [10.1016/j.apsusc.2020.145956](https://doi.org/10.1016/j.apsusc.2020.145956).
- [24] M. Iversen, M. Monisha, and S. Agarwala, "Flexible, wearable and fully-printed smart patch for pH and hydration sensing in wounds," *Int. J. Bioprinting*, vol. 8, no. 1, p. 447, Dec. 2021, doi: [10.18063/ijb.v8i1.447](https://doi.org/10.18063/ijb.v8i1.447).
- [25] O. P. Dimitriev, D. A. Grinko, Y. V. Noskov, N. A. Ogurtsov, and A. A. Pud, "PEDOT:PSS films—Effect of organic solvent additives and annealing on the film conductivity," *Synth. Met.*, vol. 159, nos. 21–22, pp. 2237–2239, Nov. 2009, doi: [10.1016/j.synthmet.2009.08.022](https://doi.org/10.1016/j.synthmet.2009.08.022).
- [26] C. Zhou, X. Zhang, N. Tang, Y. Fang, H. Zhang, and X. Duan, "Rapid response flexible humidity sensor for respiration monitoring using nano-confined strategy," *Nanotechnology*, vol. 31, no. 12, Mar. 2020, Art. no. 125302, doi: [10.1088/1361-6528/ab5cda](https://doi.org/10.1088/1361-6528/ab5cda).